Mode-Matching Analysis of Top-Hat Monopole Antennas Loaded with Radially Layered Dielectric

Laura A. Francavilla, James S. McLean, Heinrich D. Foltz, and Gentry E. Crook, *Member, IEEE*

***Abstract*— A top-hat monopole antenna with homogeneous or inhomogeneous dielectric loading over a ground plane is considered. Mode-matching analysis with proper enforcement of edge conditions is applied to the problem. The results of this technique are verified through independent calculations of admittance as well as by comparison of fields across matching regions. Measurements were also taken for comparison with the results from the model. It is shown that dielectric loading can reduce the electrical size necessary for self resonance, but only at the expense of a large increase in radiation Q.**

***Index Terms*— Antennas, dielectric loaded antennas, mode-matching methods.**

I. Introduction

ELECTRICALLY small, vertical monopole antennas operating over conducting ground planes are commonly used to generate vertically polarized, azimuthally omnidirectional fields. Such antennas generally exhibit large radiation quality factors and low radiation resistances. They are not self resonant and, therefore, require a matching network in order to be impedance matched to a source with resistive output impedance. This matching network or antenna tuner imposes serious limitations on the overall efficiency of the antenna system [1].

Top-hat loading of an electrically small vertical monopole antenna modifies the current distribution on the antenna in such a way as to decrease the radiation Q and increase the radiation resistance of the antenna [2]. In addition, material loading with dielectric and/or magnetic materials can make an electrically small antenna self resonant. The combination of top-hat loading with the use of low-loss loading materials can, therefore, produce a broad-band electrically small self-resonant antenna with a high radiation efficiency.

In this paper, the problem of a top-hat monopole antenna with inhomogeneous dielectric loading is considered. The dielectric loading, in addition to making the antenna self resonant, also makes the structure much more mechanically robust. The inhomogeneous dielectric loading considered here consists of two radial layers of dielectric. This inhomogeneity offers an additional degree of freedom in the design of such an antenna.

The presence of dielectric loading material severely complicates the application of moment-method techniques. However, the geometry of the antenna and dielectric loading are well suited for mode-matching analysis. Application of this technique is suggested by Morgan and Schwering [3], [4]. To employ mode matching, a separable geometry is required. In this case, the addition of an artificial ground plane well above the antenna structure allows the problem to be divided into cylindrical regions for which modal expansions can be readily derived. Morgan and Schwering have shown that the addition of an artificial ground plane has minimal effect on the calculated values for the input impedance and current distribution. This is true if the separation between the two ground planes l is large compared to the antenna dimensions and is selected so that the analysis frequency is not coincident with a cutoff frequency for the parallel-plate guide formed by the two ground planes. This approach is of interest since it can be applied to a larger class of antennas: antennas with geometries that can be described within a cylindrical coordinate system and which exhibit a radiation null on the z axis.

In the next section, the formulation for the electric and magnetic field expansions to be used in the mode-matching analysis will be discussed, including the boundary conditions that must be satisfied. In Section III, the mode-matching process and the resulting linear system of equations will be presented. With this, the importance of the enforcement of the field-edge condition will be discussed and the checks for the self consistency of the code presented. The results will be presented in Section IV, both from the numerical model and from antenna measurements. Antenna input impedance (radiation Q) and resonance frequency in relation to dielectric loading will be discussed.

II. Formulation

The antenna is situated over a perfectly electrically conducting (PEC) ground plane and is sandwiched by an artificial ground plane as described above. The problem can thus be divided into four regions as shown in Fig. 1. All region boundaries then coincide with constant coordinate surfaces in a cylindrical coordinate system. Cylindrical harmonic expansions are used to express electric and magnetic fields in

Manuscript received August 21, 1996; revised October 28, 1998. This work was supported by the Advanced Research Projects Agency, ARPA Contract DABT63-95-C-0077, the National Science Foundation, NSF Grant ECS-9358367, and the Henry Luce Foundation.

L. A. Francavilla, J. S. McLean, and G. E. Crook are with the Electrical and Computer Engineering Department, University of Wisconsin-Madison, Madison, WI 53706 USA.

H. D. Foltz is with the Department of Engineering, University of Texas-Pan American, Edinburg, TX 78539 USA.

Publisher Item Identifier S 0018-926X(99)02476-X.

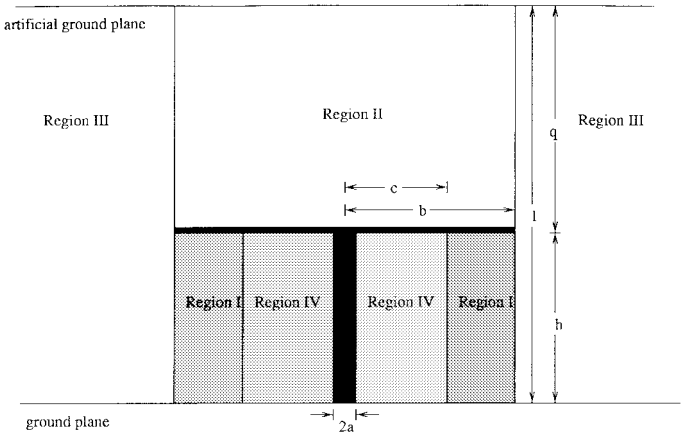

Fig. 1. Side view of top-hat loaded monopole antenna with radially layered dielectric loading.

terms of unknown weighting coefficients. The coefficients in these expansions are found by enforcing the proper boundary and continuity conditions. Currents on the antenna are then calculated from the magnetic field.

As in [3], a cylindrical coordinate system is chosen with the origin such that the lower ground plane constitutes the $z = 0$ plane and the axis of symmetry of the antenna corresponds to the z axis. The height of the antenna measured from the ground plane is h, the top-hat radius is b, and the stem radius is a. The innermost dielectric (labeled as Region IV) extends from the stem to $\rho = c$. An infinitesimal voltage-gap source [5] at the base of the stem of the antenna is used to approximate the physical situation of the antenna being driven by a coaxial line. A finite voltage-gap source used in [3] was found to yield similar results when a small gap size was used. However, the infinitesimal gap source is the better of the two approximations and has the benefits of being simpler to implement and not introduce any numerical problems into the model. An improved approximation of the coaxial feed would be a magnetic frill source [6], however, this would complicate the numerical model. Based on the agreement between the present model and experimental data (shown in Section IV) the accuracy of the infinitesimal voltage-gap source model is acceptable at lower frequencies.

A. Boundary Conditions

In the mode-matching technique, the field expansions used are weighted sums of source-free solutions to Maxwell's equations. Thus, Maxwell's equations are exactly satisfied in the interior of the regions. All that remains to be done is to enforce the boundary conditions. The tangential electric and magnetic fields must be continuous across the region boundaries. The tangential electric fields must be zero at actual and artificial ground planes and the top and bottom of the top hat because these are all assumed to be perfect electric conductors. This is accomplished by correct choice of z wavenumbers in the field expansions. Along the stem, the tangential electric field E_z is zero. Also, the top hat is assumed to be infinitesimally thin and therefore the fields at the edge of the top hat become singular. So a field edge condition, which determines how fields become singular, must be enforced. Also, to satisfy causality for a source at $\rho = 0$, there are only outward traveling waves at $\rho = \infty$.

B. Field Expansions

Following [3] and [7], the expressions for the fields of the inhomogeneous dielectric loaded top-hat monopole antenna, which follow, were derived.

The field expansions for Region I ($c \le \rho \le b$ and $0 \le z \le h$), which contains the outer layer of dielectric, are

$$E_z^I(\rho, z) = \frac{1}{j\omega\epsilon_I} \sum_{n=0}^{N_1} \gamma_n^2 [a_n H_0^{(1)}(\gamma_n \rho) + b_n H_0^{(2)}(\gamma_n \rho)] \cdot \cos\left(\frac{n\pi z}{h}\right) \quad (1)$$

$$H_\phi^I(\rho, z) = \sum_{n=0}^{N_1} \gamma_n [a_n H_1^{(1)}(\gamma_n \rho) + b_n H_1^{(2)}(\gamma_n \rho)] \cdot \cos\left(\frac{n\pi z}{h}\right) \quad (2)$$

where N_1 is the number of modes in Region I and ϵ_I is the dielectric constant of the material in Region I. $H_x^{(1)}$ are Hankel functions of the first kind and $H_x^{(2)}$ are Hankel functions of the second kind with order x of zero or one. $\gamma_n = \sqrt{\epsilon_I k_0^2 - (n\pi/h)^2}$ where γ_n are the radial wavenumbers for the nth mode and k_0 is the free-space wavenumber. a_n and b_n are the weighting coefficients to be determined. In all regions, the negative imaginary branch of the solution is chosen to satisfy causality.

In Region II, above the top hat ($\rho \le b$ and $h \le z \le l$), the field equations are

$$E_z^{II}(\rho, z) = \frac{1}{j\omega\epsilon_0} \sum_{n=0}^{N_2} c_n u_n^2 J_0(u_n \rho) \cos\left[\frac{n\pi}{q}(z - h)\right] \quad (3)$$

$$H_\phi^{II}(\rho, z) = \sum_{n=0}^{N_2} c_n u_n J_1(u_n \rho) \cos\left[\frac{n\pi}{q}(z - h)\right] \quad (4)$$

where N_2 is the number of modes in Region II. $u_n = \sqrt{k_0^2 - (n\pi/q)^2}$ where u_n is the radial wavenumber for the nth mode and $q = l - h$. c_n are weighting coefficients to be determined. J_x are Bessel functions of the first kind where the order x is zero or one.

In Region III ($\rho \ge b$ and $0 \le z \le l$) the field expansions are expressed as

$$E_z^{III}(\rho, z) = \frac{1}{j\omega\epsilon_0} \sum_{n=0}^{N_3} d_n \nu_n^2 H_0^{(2)}(\nu_n \rho) \cos\left(\frac{n\pi z}{l}\right) \quad (5)$$

$$H_\phi^{III}(\rho, z) = \sum_{n=0}^{N_3} d_n \nu_n H_1^{(2)}(\nu_n \rho) \cos\left(\frac{n\pi z}{l}\right) \quad (6)$$

where N_3 is the number of modes in Region III. $\nu_n = \sqrt{k_0^2 - (n\pi/l)^2}$ where ν_n is the radial wavenumber for the nth mode. d_n are weighting coefficients to be determined.

The field expansions for Region IV ($a \le \rho \le c$ and $0 \le z \le h$), which contains the inner layer of dielectric, are

$$E_z^{IV}(\rho, z) = \frac{1}{j\omega\epsilon_{IV}} \sum_{n=0}^{N_4} \alpha_n^2 [e_n H_0^{(1)}(\alpha_n \rho) + f_n H_0^{(2)}(\alpha_n \rho)] \cdot \cos\left(\frac{n\pi z}{h}\right) \tag{7}$$

$$H_\phi^{IV}(\rho, z) = \sum_{n=0}^{N_4} \alpha_n [e_n H_1^{(1)}(\alpha_n \rho) + f_n H_1^{(2)}(\alpha_n \rho)] \cdot \cos\left(\frac{n\pi z}{h}\right) \tag{8}$$

where N_4 is the number of modes in Region IV and ϵ_{IV} is the dielectric constant of the material in Region IV. $\alpha_n = \sqrt{\epsilon_{IV} k_0^2 - (n\pi/h)^2}$ where α_n are the radial wavenumbers for the nth mode; e_n and f_n are the weighting coefficients to be determined.

III. Mode Matching

Mode matching is accomplished by setting two field expansions equal at the boundary between them and generating a system of linear equations by taking inner products. In our formulation, Region IV shares a boundary with the source. The set of equations that results from Fourier matching along the $\rho = a$ boundary where $0 \le z \le h$ is written in terms of the e_n and f_n weighting coefficients and wavenumber α_n

$$H_0^{(1)}(\alpha_n a) e_n + H_0^{(2)}(\alpha_n a) f_n = \frac{-j2\omega\epsilon_{IV} V_0}{p_n \alpha_n^2 h} \tag{9}$$

where $n = 0, 1, \cdots, N_4$, where N_4 was chosen to be equal to N_1 and $p_0 = 2$ and $p_n = 1$ for $n \ge 1$. This is one set of equations in the complex linear system that will be used to solve for the weighting coefficients.

The continuity of tangential fields must be enforced along the $\rho = b$ boundary for four cases: enforcing the continuity of the magnetic fields in Regions I and III, Regions II and III, and then the electric fields in the same manner. The two sets of equations from the magnetic fields are combined, as are the two sets of equations resulting from matching the electric fields. These two independent expressions for the d_n weighting coefficients may be equated, eliminating the d_n coefficients. This provides a second set of equations to be used in the linear system. It is as follows:

$$\begin{aligned}
&\sum_{i=0}^{N_1} a_i \left[\frac{\gamma_i^2}{\epsilon_I} H_0^{(1)}(\gamma_i b) H_1^{(2)}(\nu_n b) - \gamma_i \nu_n H_1^{(1)}(\gamma_i b) H_0^{(2)}(\nu_n b) \right] S_{n,i} \\
&+ \sum_{j=0}^{N_1} b_j \left[\frac{\gamma_j^2}{\epsilon_I} H_0^{(2)}(\gamma_j b) H_1^{(2)}(\nu_n b) - \gamma_j \nu_n H_1^{(2)}(\gamma_j b) H_0^{(2)}(\nu_n b) \right] S_{n,j} \\
&+ \sum_{k=0}^{N_2} c_k \left[u_k^2 J_0(u_k b) H_1^{(2)}(\nu_n b) - u_k \nu_n J_1(u_k b) H_0^{(2)}(\nu_n b) \right] T_{n,k} = 0
\end{aligned} \tag{10}$$

where $n = 0, 1, \cdots, N_3$. The value of N_3 was chosen to be $N_1 + N_2$ in order to obtain the same number of equations as unknown weighting coefficients and to satisfy the edge condition described below. $S_{n,m}$ and $T_{n,m}$ are integrals which result from the mode matching and are given by

$$S_{n,m} = \int_0^h \cos\left(\frac{n\pi}{l} z\right) \cos\left(\frac{m\pi}{h} z\right) dz \tag{11}$$

and

$$T_{n,m} = \int_h^l \cos\left(\frac{n\pi}{l} z\right) \cos\left(\frac{m\pi}{q}(z-h)\right) dz. \tag{12}$$

Two other sets of equations arise from matching tangential electric and magnetic fields at the $\rho = c$ boundary between Regions IV and I. From matching corresponding electric fields, we have

$$\frac{1}{\epsilon_I} \gamma_n^2 [a_n H_0^{(1)}(\gamma_n c) + b_n H_0^{(2)}(\gamma_n c)] = \frac{1}{\epsilon_{IV}} \alpha_n^2 [e_n H_0^{(1)}(\alpha_n c) + f_n H_0^{(2)}(\alpha_n c)] \tag{13}$$

where $n = 0, 1, \cdots, N_1$. The magnetic fields are matched in the same manner, yielding

$$\gamma_n [a_n H_1^{(1)}(\gamma_n c) + b_n H_1^{(2)}(\gamma_n c)] = \alpha_n [e_n H_1^{(1)}(\alpha_n c) + f_n H_1^{(2)}(\alpha_n c)] \tag{14}$$

where $n = 0, 1, \cdots, N_1$. The complex linear system of order $4N_1 + N_2 + 5$ is comprised of these two sets of equations and those from (9) and (10). The right-hand side of the matrix system is zero except for the $N_1 + 1$ driving terms from (9). Solving the linear system will now yield the a_n, b_n, c_n, e_n, and f_n coefficients. Knowing these, the d_n coefficients are easily found. The known coefficients are then substituted into the expressions for the electric and magnetic fields, which are then used to calculate other quantities of interest such as current and energy.

It might seem necessary to include another equation in the linear system in order to force the total radially directed current at the rim of the top hat to zero as in the "null current condition" in [3], but to do so is superfluous. This will be addressed in the next subsection.

A. Edge Condition

To obtain convergent results it is desirable to be able to increase the number of modes in the field expansions. Doing so requires a well-conditioned set of equations. In [3], a "null current condition" was applied which requires

$$H_\phi^I(\rho = b, z = h) = H_\phi^{II}(\rho = b, z = h). \tag{15}$$

This is equivalent to forcing the radial current on the top hat to zero at its rim. However, to properly carry out mode matching, the magnetic fields in Regions I and II should each join continuously with the magnetic field in Region III in the limit as the number of modes becomes large. This ensures that the null current condition will be satisfied automatically in the same limit.

It is well known [8] that the number of modes in mode-matching analysis cannot be chosen arbitrarily. In particular,

the ratio of the number of modes used in adjoining regions must be chosen correctly. From the viewpoint of electromagnetic field expansions, this ratio ensures that the summations, in the limit of a large number of terms, have the correct order of singularity approaching the edge. The rigorous derivation of the edge condition in [8] applied to a bifurcation in a rectangular waveguide also applies to the geometry in our case. The resulting edge condition is

$$\frac{N_2}{N_1} = \frac{q}{h} \tag{16}$$

where $N_1 + N_2 = N_3$.

This constraint on the number of modes can also be determined, though less rigorously, by examining the inner products generated when matching high-order modes at the boundaries. The product of two sinusoids integrated over many periods will be very small unless the periods are nearly identical. If one expands a single high-order mode in one region in terms of the modes in the adjoining region, one sees that most of the "matching" is done by the one or two modes of the adjoining region that have the closest spatial frequency. Thus, if the highest order modes in two adjacent regions do not have nearly the same period, the coefficient for the one with the larger number of periods will be poorly determined and the problem will be ill conditioned.

To obtain a close match of periods between Regions I and III, it is required that

$$\frac{N_3}{l} = \frac{N_1}{h}. \tag{17}$$

To obtain a close match of periods between Regions II and III it is required that

$$\frac{N_3}{l} = \frac{N_2}{q}. \tag{18}$$

These two conditions are combined resulting in (16) above. Hence, we believe that (15) is superfluous and (16) should be used instead.

The total number of modes N_3 must be chosen. A general rule of thumb for determining N_3 is to include the lowest order mode under the structure plus at least one evanescent mode. This suggests the following rule: $N_3 > h/(\lambda/2)$. If the value of N_3 is too low, the results will not converge. Choosing a value of N_3 that is too large results in an ill-conditioned matrix. We found it possible to include four to eight times the value of $h/(\lambda/2)$ for N_3.

B. Self-Consistency Checks

The self consistency of our mode-matching algorithm was evaluated using two methods. First, a comparison was performed between input admittance of the monopole as computed directly from the stem current at the gap source and as computed via the conservation of complex power. The input admittance as computed from the stem current is

$$Y = \frac{I(d)}{V_0} = 2\pi a H_\phi^I(a, d). \tag{19}$$

The input impedance as computed via the conservation of complex power is [7]

$$Y = \frac{2P_{\text{in}}^*}{|V_0|^2} = \frac{2}{|V_0|^2}\left[P_{\text{rad}} - j2\omega(W_e - W_m)\right] \tag{20}$$

where P_{rad} is the radiated power and W_e and W_m are the time average stored electric and magnetic energies, respectively. The first term in (20) (the conductance) can be computed from the surface integral of the real part of the Poynting vector over a surface enclosing the antenna. Taking this surface to be a cylinder in Region III, we obtain

$$P_{\text{rad}} = \frac{2\pi}{\omega\epsilon_0}\sum_{n=0}^{N_3} g_n |d_n|^2 |\nu_n|^3 \cdot \left[J_0(\nu_n\rho)N_1(\nu_n\rho) + N_0(\nu_n\rho)J_1(\nu_n\rho)\right]. \tag{21}$$

The second term in (20) (the susceptance) involves the computation of the difference between the time-average stored electric and magnetic energy around the antenna. The total energy in Region III is infinite due to the steady-state nature of the problem. Nevertheless, the quantity $W_e - W_m$ is finite. After some manipulation, the expression for $W_e - W_m$ in Region III can be shown to be

$$W_e - W_m = \frac{\pi}{2\omega^2\epsilon_0}\int_b^\infty \sum_{n=0}^{N_3} g_n |d_n|^2 |\nu_n|^4 \cdot \left[\left([J_0(\nu_n\rho)]^2 + [N_0(\nu_n\rho)]^2\right) - \left([J_1(\nu_n\rho)]^2 + [N_1(\nu_n\rho)]^2\right)\right] \rho\, d\rho \tag{22}$$

where g_n is l when $n = 0$ and $l/2$ when $n > 0$. This makes use of energy orthogonality of the modes, which follows from the orthogonality of the circular sine and cosine functions. When the asymptotic forms of the Bessel and Neumann functions are used, the integrand is identically zero, which is in keeping with the equipartition of energy in the far field. Evaluation of the integral therefore yields

$$W_e - W_m = \frac{\pi}{2\omega^2\epsilon_0}\sum_{n=0}^{N_3} g_n |d_n|^2 |\nu_n|^4 \cdot \left[\frac{b}{\nu_n}\left(J_0(\nu_n b)J_1(\nu_n b) + N_0(\nu_n b)N_1(\nu_n b)\right)\right]. \tag{23}$$

Similar expressions can be derived for all regions.

As an example, these computations were performed for an unloaded monopole with the same dimensions as that used in [3]. Fig. 2 shows plots of both susceptance and conductance versus frequency calculated from energy and current when the edge condition is properly enforced. The good agreement between susceptance curves suggests the self-consistency of the code. When the null current condition is enforced instead of the edge condition, however, the agreement is quite poor. Since conductance is calculated from far-field radiated power, which is relatively insensitive to perturbations, it is expected to be better behaved than the susceptance. There is still, however, an improvement in the level of agreement when the edge condition is enforced. Conductance calculations were in agreement to at least six decimal places when the field edge condition was enforced. If the null current condition is enforced instead, there is agreement between the two

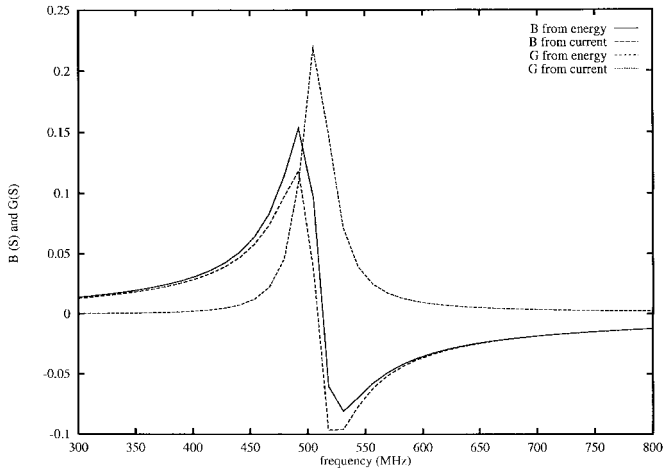

Fig. 2. Comparison of susceptance and conductance independently calculated from current- and time-average stored energies as a function of frequency when the field-edge condition is enforced. The dimensions of the antenna were $a = 1.19$ mm, $b = 3.87$ cm, and $h = 3.175$ cm.

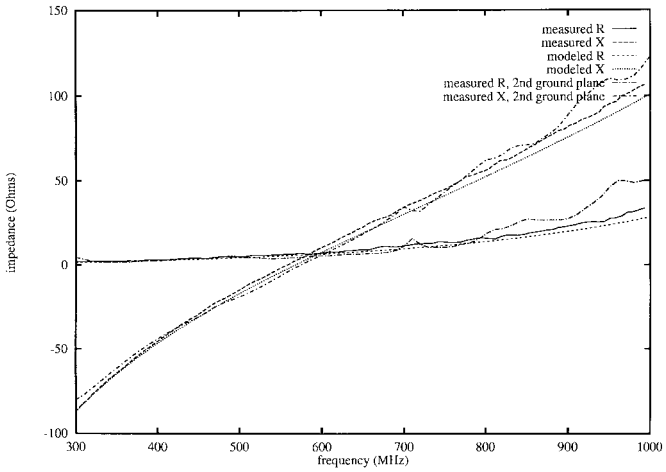

Fig. 4. Comparison of input impedance from experiment and from model as a function of frequency for the unloaded top-hat monopole antenna. The dimensions of the antenna are $a = 2.381$ mm, $b = 3.810$ cm, and $h = 3.200$ cm.

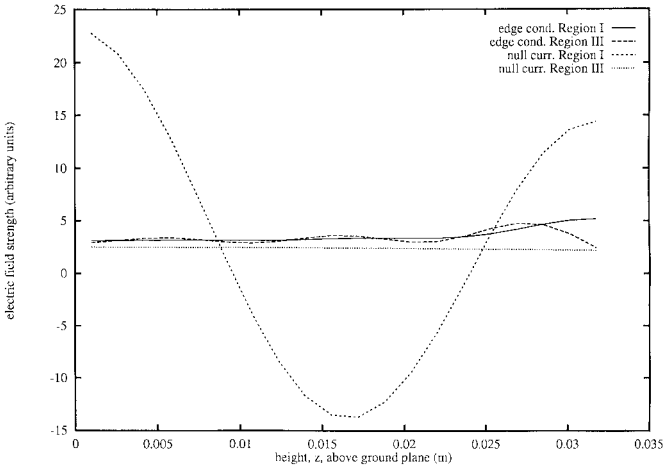

Fig. 3. Comparison of the strength of the imaginary component of the z-directed electric fields at $\rho = b$ boundary as a function of height when the field edge condition is enforced and when the null current condition is enforced. Similar behavior was observed for the real components of these fields. The dimensions of the antenna are the same as those in Fig. 2.

calculations to only two decimal places. A second check on the self-consistency of the algorithm involved verification of the continuity of the computed electric and magnetic fields at the region boundaries. The real and imaginary components of the electric and magnetic fields were plotted as a function of height z showing the fields matching across cylindrical regions. For the unloaded monopole used in [3], Fig. 3 shows the imaginary component of both E_z^I and E_z^{III} on the $\rho = b$ boundary for both the field and null current conditions. The agreement between the two is clearly much better when the edge condition is enforced than when the null current condition is enforced without the edge condition. This was also the case for the real components of these electric fields.

C. Numerical Efficiency and Limitations of the Algorithm

Because all of the matrix inner products are obtainable in closed form, no numerical integration is required to set up the linear system. Also, because the mods used in each region are analogous to the "entire-domain" basis functions used in moment-method techniques, a relatively small number of them is required to obtain accurate results. This was also noted in [3]. Thus, it is expected that this approach is at least as efficient as moment-method techniques.

The main limitation of this mode-matching algorithm is the fact that it only applies to a limited set of geometries—separable, cylindrical geometries, for which no power radiates along the z axis. Nevertheless, there are many geometries to which this method can be applied. This algorithm can include the effects of dielectric loss via the use of a complex permittivity. Conductive losses require more effort to include in that the field expansions must be made more general. A more comprehensive model with both types of losses is currently under development.

IV. Results and Experimental Verification

The numerical model discussed above was used to model several different top-hat monopole antennas, loaded and unloaded, and the results were verified with experiments. The monopole antennas were constructed out of copper and fed through a bulkhead connector in a ground plane. Input impedance measurements were made with an automatic vector network analyzer.

1) Unloaded Monopole: In Fig. 4, the predicted and measured input impedance of an unloaded top-hat monopole with dimensions $a = 2.381$ mm, $b = 3.810$ cm, and $h = 3.200$ cm are shown. The resistance curves show excellent agreement while the reactance curves, although still in good agreement, tended to diverge somewhat at higher frequencies. These measurements were repeated with a second ground plane placed above the antenna as was assumed in the numerical model. The results for a ground plane spacing of 23 cm (the smallest distance assumed in the numerical model) are shown in Fig. 4. As can be seen, the second ground plane had a very small effect on the data.

2) Teflon-Loaded Monopole: A Teflon-loaded top-hat monopole was also characterized; the results are shown in

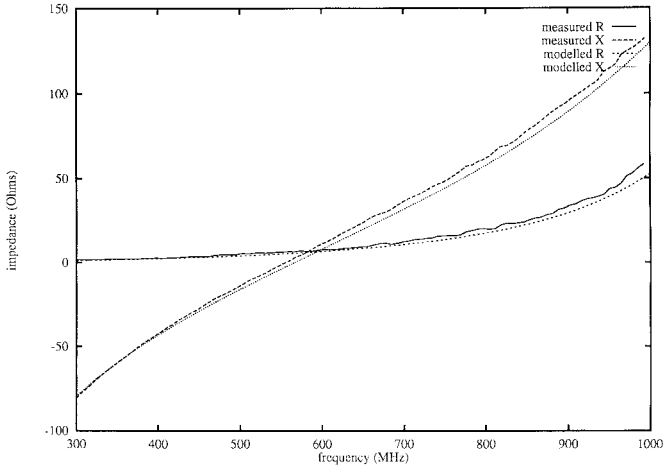

Fig. 5. Comparison of input impedance from experiment and from model as a function of frequncy for the Teflon-loaded top-hat monopole antenna. The dimensions for this antenna are the same as those in Fig. 4 except that $c = 1.27$ cm.

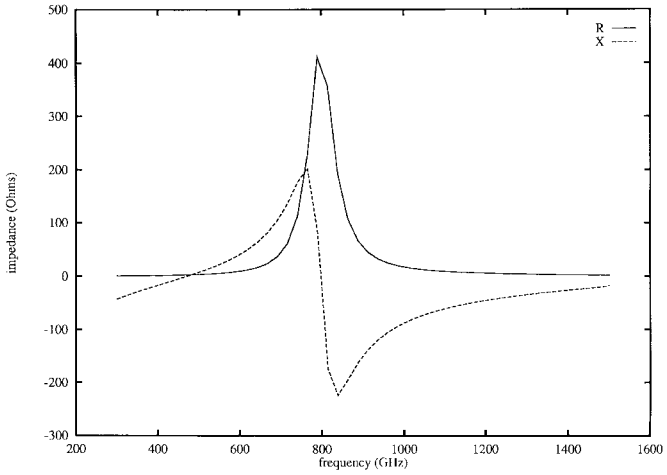

Fig. 6. Plot of calculated input impedance as a function of frequency for the top-hat monopole antenna with dielectric loading in Region IV with $\epsilon_{IV} = 10.0$. The dimensions of the antenna are the same as those in Fig. 4 except that $c = 1.5$ cm.

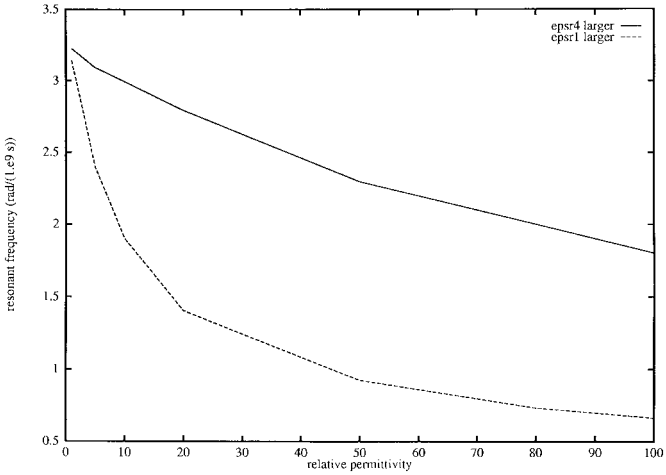

Fig. 7. First-series resonance frequency as a function of relative permittivity. The solid line represents dielectric loading in Region IV and air in Region I. The dashed line represents dielectric loading in Region I and air in Region IV. All antennas had the dimensions specified in Fig. 4.

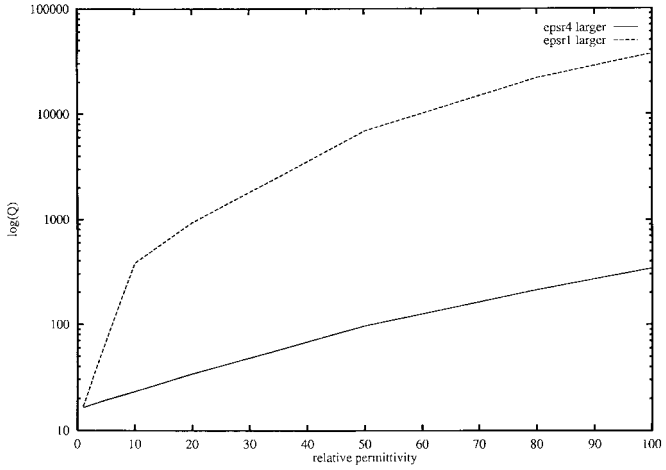

Fig. 8. $\log(Q)$ as a function of relative permittivity. The solid and dashed lines represent the same situations given in Fig. 7. All antennas had the dimensions specified in Fig. 4.

Fig. 5. The dielectric loading of the antenna was inhomogenous as Teflon was placed only in Region IV. The dimensions for this antenna were the same as those given for the unloaded top-hat monopole antenna with $\epsilon_{IV} = 2.1$ and $c = 1.27$ cm. The shift in resonance frequency was small as expected, but correctly predicted. Again, the experimentally determined and computed resistance curves agree quite well and the reactance curves show fairly good agreement.

3) Monopole Loaded with High-Density Dielectric: The effect of a high-density dielectric in Region IV was investigated using the numerical model. For this study, the following monopole dimensions were chosen: $a = 1.19$ mm, $b = 3.870$ cm, $c = 1.500$ cm, and $h = 3.175$ cm. For the particular case of $\epsilon_{IV} = 10.0$ and $\epsilon_I = 1.0$, the predicted input impedance is plotted in Fig. 6 showing a significant reduction of the fundamental resonance frequency.

In order to study the size reduction obtained by dielectric loading, the fundamental resonance frequency of a loaded monopole with the above dimensions was plotted versus ϵ_R as in Fig. 7. The solid line indicates the situation where ϵ_{IV}, the innermost dielectric layer, is varied and ϵ_I is held fixed at 1.0. The dashed line indicates the opposite case with ϵ_I varied over a range of values and ϵ_{IV} constant at 1.0. It can be seen that loading the antenna with material of higher dielectric constant will decrease the resonance frequency, ω_0. However, this dielectric loading also increases the Q tremendously. The radiation Q (approximately twice the inverse of fractional impedance bandwidth) was calculated at the first-series resonance for increasing dielectric constants. The expression for Q can be derived from energy and power [7]

$$Q = \frac{\omega L}{R} = \frac{\left(X + \omega \dfrac{\partial X}{\partial \omega}\right)}{2R}. \tag{24}$$

A plot of $\log Q$ versus ϵ_r is shown in Fig. 8. Again, the solid line indicates the situation where ϵ_{IV} is large and ϵ_I is constant

at 1.0. The dashed line indicates the opposite, with ϵ_I varied over a range of values and ϵ_{IV} constant at 1.0.

V. Conclusion

The technique of mode matching was applied to a top-hat loaded monopole antenna, which may have homogeneous or inhomogeneous loading under the top-hat structure. Because the matrix inner products are available in closed form, the technique is comparable to moment methods in the required numerical effort, but can be applied to geometries difficult to analyze by moment methods. The separable, cylindrical geometry of the structure lends itself to mode matching, which provides an accurate analysis for this geometry. In contrast to previous work, it was shown that to obtain good results the edge condition must be properly enforced and the null current condition must not be used. Measurements were taken for comparison with numerical results in some cases and showed good agreement. It was also shown that the series resonance frequency ω_0 can be reduced by using dielectric loading. However, this is done at the expense of increased Q, much higher than would be expected from the decrease in electrical size.

Acknowledgment

The authors would like to thank J. Casey, K. Dorner, and L. Rauth of the Electrical and Computer Engineering Department, University of Wisconsin-Madison for their assistance with the experimental work.

References

[1] G. S. Smith, "Efficiency of electrically small antennas combined with matching networks," *IEEE Trans. Antennas Propagat.*, vol. AP-25, pp. 369–373, May 1977.
[2] A. F. Gangi, S. Sensiper, and G. R. Dunn, "The characteristics of electrically short, umbrella top-loaded antennas," *IEEE Trans. Antennas Propagat.*, vol. AP-13, pp. 864–871, Nov. 1965.
[3] M. A. Morgan and F. K. Schwering, "Eigenmode analysis of dielectric loaded top-hat monopole antennas," *IEEE Trans. Antennas Propagat.*, vol. 42, pp. 54–61, Jan. 1994.
[4] M. A. Morgan, R. C. Hurley, and F. K. Schwering, "Computation of monopole antenna currents using cylindrical harmonics," *IEEE Trans. Antennas Propagat.*, vol. 38, pp. 1130–1133, July 1990.
[5] C. A. Balanis, *Antenna Theory*, 2nd ed. New York: Wiley, 1997.
[6] L. L. Tsai, "A numerical solution for the near and far fields of an annular ring of magnetic current," *IEEE Trans. Antennas Propagat.*, vol. AP-20, pp. 569–576, Sept. 1972.
[7] R. F. Harrington, *Time-Harmonic Electromagnetic Fields.* New York: McGraw-Hill, 1961.
[8] R. Mittra and S. W. Lee, *Analytical Techniques in the Theory of Guided Waves.* New York: Macmillian, 1971.

Laura A. Francavilla received the B.A. degree in physics from Oberlin College, Oberlin, OH, in 1995, and the M.S. degree in electrical engineering from the University of Wisconsin-Madison, in 1997.

Since 1997, she has been employed by the Hewlett-Packard Company at the Santa Rosa Systems Division (SRSD), Santa Rosa, CA.

James S. McLean received the B.S., M.S., and Ph.D. degrees in electrical engineering from the University of Texas at Austin, in 1984, 1986, and 1990, respectively.

He worked for TRW Antenna Systems Laboratory, Redondo Beach, CA, and for the University of Wisconsin-Madison, where he performed research in the area of electrically small and low-profile antennas for wireless and mobile communications. He is currently a Research Associate at the University of Texas-Pan American, Edinburg, where he is continuing research in this area.

Heinrich D. Foltz received the B.S.E.E., M.S.E., and Ph.D. degrees in electrical engineering from the University of Texas at Austin.

He was employed at Applied Research Laboratories, Austin, TX, from 1992 to 1994, and is currently an Assistant Professor at the University of Texas-Pan American, Edinburg.

Gentry E. Crook (S'80–M'89) received the B.S., M.S., and Ph.D. degrees in electrical engineering from the University of Texas at Austin in 1984, 1986, and 1989, respectively.

She was a Visiting Scientist at the Max Planck Institute for Solid State Studies, Stauttgart, Germany, and then an Assistant Professor of Electrical Engineering, University of Wisconsin-Madison. Her graduate work interests involved growth and processing of compound semiconductor materials for high-performance transistors and optoelectronic devices. She has coauthored more than 20 publications in referred electical engineering and physics journals and presented numerous conference papers and seminars.

Dr. Crook received a Teaching Award from the Student Engineering Council, University of Wisconsin. She is a member of the Eta Kappa Nu, Tau Beta Pi, and Sigma Xi honor societies. She is also a member of the Institute of Electical and Electronics Engineers, the American Physical Society, the American Vacuum Society, and the Materials Research Society.